UC San Diego
UC San Diego Previously Published Works

Title

Mechanical Disruption of the Inner Limiting Membrane In Vivo Enhances Targeting to the Inner Retina

Permalink

https://escholarship.org/uc/item/0d05f7ft

Journal

Investigative Ophthalmology & Visual Science, 64(15)

ISSN

0146-0404

Authors

L., Jiun

Pedroarena-Leal, Nicole

Louie, Mikaela

et al.

Publication Date

2023-12-20

DOI

10.1167/iovs.64.15.25

Copyright Information

Peer reviewed

Mechanical Disruption of the Inner Limiting Membrane In Vivo Enhances Targeting to the Inner Retina

Jiun L. Do,[1] Nicole Pedroarena-Leal,[1] Mikaela Louie,[2] Paula Avila Garcia,[1] Adam Alnihmy,[1] Amit Patel,[1] Robert N. Weinreb,[1] Karl J. Wahlin,[1] Anna La Torre Vila,[2] and Derek S. Welsbie[1]

[1]Gleiberman Center for Glaucoma Research, Hamilton Glaucoma Center, Shiley Eye Institute and Viterbi Family Department of Ophthalmology, University of California San Diego, La Jolla, California, United States
[2]Department of Cell Biology and Human Anatomy, University of California Davis, California, United States

PURPOSE. To evaluate the effects of mechanical disruption of the inner limiting membrane (ILM) on the ability to target interventions to the inner neurosensory retina in a rodent model. Our study used an animal model to gain insight into the normal physiology of the ILM and advances our understanding of the effects of mechanical ILM removal on the viral transduction of retinal ganglion cells and retinal ganglion cell transplantation.

METHODS. The ILM in the in vivo rat eye was disrupted using mechanical forces applied to the vitreoretinal interface. Immunohistology and electron microscopy were used to verify the removal of the ILM in retina flatmounts and sections. To assess the degree to which ILM disruption enhanced transvitreal access to the retina, in vivo studies involving intravitreal injections of adeno-associated virus (AAV) to transduce retinal ganglion cells (RGCs) and ex vivo studies involving co-culture of human stem cell–derived RGCs (hRGCs) on retinal explants were performed. RGC transduction efficiency and transplanted hRGC integration with retinal explants were evaluated by immunohistology of the retinas.

RESULTS. Mechanical disruption of the ILM in the rodent eye was sufficient to remove the ILM from targeted retinal areas while preserving the underlying retinal nerve fiber layer and RGCs. Removal of the ILM enhanced the transduction efficiency of intravitreally delivered AAV threefold (1380.0 ± 290.1 vs. 442.0 ± 249.3 cells/mm^2; $N = 6$; $P = 0.034$). Removal of the ILM was also sufficient to promote integration of transplanted RGCs within the inner retina.

CONCLUSIONS. The ILM is a barrier to transvitreally delivered agents including viral vectors and cells. Mechanical removal of the ILM is sufficient to enhance access to the inner retina, improve viral transduction efficiencies of RGCs, and enhance cellular integration of transplanted RGCs with the retina.

Keywords: inner limiting membrane, inner limiting membrane peel, adeno-associated virus, stem cells, retinal ganglion cells, retinal ganglion cell direct cell replacement, retinal ganglion cell integration, optic nerve regeneration

Ophthalmologic diseases such as glaucoma and other optic neuropathies cause the loss of retinal ganglion cells (RGCs). RGC loss results in the loss of axonal connections between the retina and central vision-associated targets necessary for vision. Because RGCs do not spontaneously regenerate, the loss of RGCs results in permanent vision loss.[1,2] To preserve or restore vision, RGCs must be protected following injury or replaced when they are lost.

Stem cells are a potential source of replacement cells and can be directed to become RGCs. RGCs derived from human pluripotent stem cells (hRGCs) express RGC-enriched genetic and phenotypic markers and demonstrate electrophysiological activity that is similar to that of endogenous RGCs.[3–6] RGCs transplanted into rodent eyes through intravitreal injections integrate into the neurosensory retina and can extend axons to central targets in the brain.[7–10] However, the rates of successful cellular integration per injection are modest at best. A possible reason for this limited success is that the inner limiting membrane (ILM) is a physical barrier between the vitreous and the inner retina. The ILM is also a barrier to virus-mediated interventions targeting the retina using intravitreal injections.[11]

The ILM is comprised of laminin, collagen, and other extracellular matrix protein.[12–14] Developmentally, it is essential for the proper migration of cells from the outer to inner retinal layers and preventing retinal cells from migrating into the vitreous.[15] In the adult, the function of the ILM is unclear. It may protect the inner retina from internal forces, but it also acts as a barrier that prevents intravitreally transplanted cells from migrating into the neuroretina and integrating with existing retinal circuits.[16] Enzymatic removal of the ILM can enhance the degree to which

transplanted RGCs integrate with a host retina.[17] However, proteases do not specifically target the ILM, and off-target results can occur. Additionally, the narrow therapeutic window of proteases limits their clinical viability. A more clinically translatable approach is needed to remove the ILM.

Clinically, mechanical removal of the ILM is performed during vitreoretinal surgery for macular holes, epiretinal membranes, and other vitreomaculopathies.[18] Although peeling the ILM may improve visual acuity and/or reduce metamorphopsia, there are potential risks such as histological changes in the retina from trauma and microscotomas.[19] Further, it is uncertain whether mechanical removal of the ILM is sufficient to enhance access of intravitreally introduced agents to the neuroretina. In this study, we evaluated whether mechanical removal of the ILM in a rodent model is sufficient to enhance access of intravitreally delivered viral vectors to the neurosensory retina and to permit the integration of transplanted RGCs.

MATERIALS AND METHODS

Animals

All animal use adhered to the ARVO Statement for the Use of Animals in Ophthalmic and Vision Research. Protocols were reviewed and approved by the Veterans Affairs San Diego Healthcare System Institutional Animal Care and Use Committee (IACUC). Sprague Dawley rats 7 to 8 weeks of age were obtained from Envigo (Placentia, CA, USA). Transgenic Fischer 344 rats that ubiquitously express green fluorescent protein (GFP) under the ubiquitin C (*UBC*) promoter and were 7 to 8 weeks of age were obtained for an in-house breeding colony (Rat Resource and Research Center, University of Missouri, Columbia, MO, USA).

Disruption of the ILM in Adult Rats In Vivo

Animals were anesthetized with an intramuscular injection of anesthetic comprised of ketamine (75 mg/kg) and medetomidine (0.5 mg/kg). Following confirmation of a deep anesthetic state with a lack of response to toe pinch, the animal was positioned in the lateral decubitus position. A drop of 0.5% proparacaine was administered to the rodent eye, and the eye was sterilized with a 5% povidone–iodine solution. Ophthalmic hydroxypropyl methylcellulose 0.3% ointment was applied to the cornea and a glass coverslip placed over the cornea. Proptosis of the eye was induced, and a temporal sclerotomy was made with a 23-gauge needle. A 25-gauge micro-serrated nitinol loop (Alcon, Fort Worth, TX, USA) was introduced through the sclerotomy, and the loop extended into the vitreous cavity. Under direct visualization of the nasal retina, at least five passes against the retinal surface were made using the loop. The amount of force applied was adjusted by varying the extent to which the loop was extended and was inversely correlated with the degree of extension. In some cases, accumulations of tissue along the serrated edges of the loop could be appreciated. The loop was then retracted, and the instrument was removed from the eye. Erythromycin 0.5% ophthalmic ointment was applied to the eye. The animals received intramuscular injections of the reversing anesthetic agent atipamezole (1 mg/kg) and were monitored until recovery from anesthesia.

Intravitreal Adeno-Associated Virus Injections

One week following the mechanical disruption of the ILM, animals were anesthetized, and the eyes were prepared for surgery as described above. A 32-gauge point style 2 needle on a Hamilton syringe (Hamilton Company, Reno, NV, USA) was used to penetrate the globe posterior to the nasal limbus and inject 5 µL of virus into the vitreous cavity. Adeno-associated virus (AAV) serotype 2 (AAV2) expressing GFP driven by a CAG promoter was delivered at a titer of 1E11 vector genomes (vg)/mL. The needle was maintained within the vitreous cavity for 30 seconds before it was removed to prevent reflux. Erythromycin 0.5% ophthalmic ointment was applied to the eye. Anesthesia was reversed, and animals were monitored until recovery.

Adult Rat Retinal Explants

Adult retinal explants were prepared according to the protocol described by Johnson et al.[20,21] Briefly, animals were anesthetized with an intramuscular injection of ketamine (50 mg/kg), xylazine (2.6 mg/kg), and acepromazine (0.5 mg/kg). When the animal was nonresponsive to toe pinch, the globe was enucleated and transferred to cold Hank's Balanced Salt Solution containing calcium and magnesium (Thermo Fisher Scientific, Waltham, MA, USA), and the animal was euthanized. An incision through the sclera was made immediately posterior to the limbus, and the cornea was removed by continuing the incision circumferentially along the posterior limbus. The lens and vitreous were removed from the eye cup. The retina was carefully dissected free from the sclera, and the optic nerve was cut flush with the scleral wall. The retinas were cut into quadrants and transferred onto 12-mm polytetrafluoroethylene (PTFE) 0.4-µm cell culture inserts (MilliporeSigma, Burlington, MA, USA) using a plastic transfer pipette with the inner retina directed apically. Excess fluid in the insert was removed with a pipette, and the insert was transferred to a 12-well plate with a medium comprised of Neurobasal-A (Thermo Fisher Scientific), 2% B-27 supplement (Thermo Fisher Scientific), 1% N-2 supplement (Thermo Fisher Scientific), 2-mM GlutaMAX (Thermo Fisher Scientific), and penicillin–streptomycin (100 U/mL–100 µg/mL; Thermo Fisher Scientific). Half of the medium was exchanged every other day.

Human Induced Pluripotent Stem Cell–Derived RGCs

All studies with stem cells were carried out with the approval of the institutional review board (IRB) of the University of California San Diego with IRB and Stem Cell Research Oversight Committee approval. Induced pluripotent stem cells (iPSCs) were derived from peripheral blood mononuclear cells and genetically edited and differentiated into hRGCs as described in Patel et al.[22] Briefly, iPSCs genetically modified to express tdTomato and mouse CD90.2/Thy1.2 at the *POU4F2* (*BRN3B*) locus were plated on Matrigel-coated plates in mTeSR1 with 5-mM blebbistatin. The day after plating, the medium was completely changed to a differentiation medium, comprised of Gibco Dulbecco's Modified Eagle Medium/Nutrient Mixture F-12 (DMEM/F-12) and Neurobasal 1:1 medium supplemented with Gibco GlutaMAX, 5% antibiotic–antimycotic, 1% Sato, and 2% Neuronal Supplement 21 (NS21), followed by incubation in normoxic conditions (5% CO_2/20% O_2 at 37°C). The medium was

completely changed every other day with differentiation medium supplemented with forskolin (25 μM), IWR-1 (2.5 μM), dorsomorphin (1 μM), and nicotinamide (1 M) from days 1 to 6; forskolin (25 μM) and nicotinamide (1 M) from days 7 to 10; forskolin (25 μM) from days 11 to 17; and forskolin (25 μM) and dual antiplatelet therapy (DAPT; 10 μM) from days 18 to 30. Cells were periodically tested for mycoplasma contamination by polymerase chain reaction.[23]

Purification of human RGCs was accomplished according to the protocol for the EasySep Mouse CD90.2 Positive Selection Kit II (STEMCELL Technologies, Cambridge, MA, USA). Briefly, differentiated cultures were dissociated into a single-cell suspension. Cultures were washed with PBS without calcium or magnesium, incubated with Gibco TrypLE Express (Thermo Fisher Scientific) for 15 minutes at 37°C, and then further incubated with Invitrogen Accumax (Thermo Fisher Scientific) for an additional 45 minutes. The cell suspension was centrifuged, the pellet was resuspended in PBS supplemented with BSA and insulin, and the single-cell suspension was passed through a 30-μm cell strainer. The cell suspension was then combined with mouse anti-CD90.2 antibody conjugated beads and incubated at room temperature for 3 minutes in a round-bottom tube on an EasySep magnet (STEMCELL Technologies). The supernatant was removed with the tube on the magnet. The tube was removed from the magnet, the cells were washed with autoMACS Rinsing Solution (Miltenyi, Bergisch Gladbach, Germany) with 2% fetal bovine serum, and the tube was returned to the magnet. Washes were repeated 8 to 10 times. The cells were resuspended in retinal explant media. Purified hRGCs (2000 cells) were directly plated in a minimal volume of medium (2 μL) as a droplet onto the inner retina of the retinal explants prepared the same day.

Retina Histology

Animals were perfused with PBS followed by 4% paraformaldehyde (PFA). The globes were enucleated and fixed in 4% PFA overnight, and the retinas were extracted. Orientation of the retina was maintained with an incision in the temporal retina. To prepare retinal cross-sections, retinas were embedded in optimal cutting temperature compound (Scigen Scientific, Gardena, CA, USA). Embedded retinas were cut on a cryostat (10 μm) and directly mounted onto Superfrost Plus microscope slides (Thermo Fisher Scientific). Every sixth section was processed for analysis. For retinal explants, cell culture inserts were fixed with 4% PFA overnight at 4°C, and the membrane was excised from the insert.

Fixed specimens were washed in PBS with 0.25% Triton X-100, then blocked in 10% donkey serum for 1 hour at room temperature. Retinas and retina explants were incubated with primary antibodies in blocking solution for 3 to 5 days at 4°C. Retina sections were incubated in primary antibody overnight at 4°C. The primary antibodies used were specific for gamma-synuclein (SNCG) (1:500; Abnova, Walnut, CA, USA), GFP (1:1000; Aves Labs, Davis, CA, USA), laminin (1:1000, MilliporeSigma; 1:1000, Abcam, Cambridge, UK), mCherry (1:1000; Sicgen, Cantanhede, Portugal), and CD11b (1:250; Abcam). Retinas were rinsed with PBS and incubated in secondary antibody (1:1000; Thermo Fisher Scientific) overnight at 4°C. Retinas were flattened and mounted on slides. Slides were coverslipped with Mowiol (Sigma-Aldrich, St. Louis, MO, USA) and left to dry overnight.

For transmission electron microscopy, the corneas of enucleated globes were perforated, and the globes were fixed with 2% glutaraldehyde and 2.5% formaldehyde in 0.1-M cacodylate buffer (pH 7.4) for 12 hours at room temperature. The specimens were transferred to PBS, washed with 0.1-M cacodylate buffer, and postfixed in 1% osmium tetroxide for 2 hours at room temperature. The retinas were then dehydrated in a graded ethanol series, further dehydrated in propylene oxide, and embedded in EPON epoxy resin. Semithin (1 μm) and ultrathin sections were cut with a Leica EM UC6 ultramicrotome (Leica Microsystems, Leica, Germany) and collected on pioloform-coated (Ted Pella, Redding, CA, USA) one-hole slot grids. Sections were contrasted with Reynolds lead citrate and 8% uranyl acetate in 50% ethanol. Images were captured on a Philips CM120 electron microscope (Philips, Amsterdam, the Netherlands) equipped with an AMT BioSprint side-mounted digital camera and AMT Capture Engine software (AMT Imaging, Woburn, MA, USA).

Retinal Imaging and Quantification

Images of flatmounted retinas and retina cross-sections were acquired using a ZEISS Axioscan microscope with a 10× objective (Carl Zeiss Meditec, Oberkochen, Germany). Fluorescent images of the retina were acquired with a Z-stack. Shading correction was applied to each image, and Z-stacks were flattened using maximum projections. Images were stitched together to generate images of the entire retina. Confocal images of retina explants were acquired using an Olympus FV3000 confocal microscope (Olympus, Tokyo, Japan).

The density of either GFP-expressing or SNCG-positive RGCs was quantified manually using ImageJ (National Institutes of Health, Bethesda, MD, USA) by investigators masked to the experimental conditions. At least six replicates were included in each experimental group. For quantification over the entire retina, four fields (each measuring 500 μm × 500 μm with two fields 2 mm from the optic disc and two fields 1 mm from the optic disc) in each quadrant (16 fields total) of the retina were specified. The densities of immune-positive cells (cells per mm^2) were averaged over all the fields in each retina and then averaged over all subjects in each experimental group. For quantification over a focal area of the retina, a 500 μm × 500 μm field centered over the highest GFP-expressing area in the nasal retina was identified. Immunopositive cell densities (cells per mm^2) were quantified in a single field and then averaged over all subjects in each experimental group.

GFP- or SNCG-immunolabeling intensity in RGCs from retina flatmounts was quantified using ImageJ. The mean pixel intensity was determined from the focal field corresponding to the area with the highest GFP expression from each retina or from the average of 16 fields used to quantify RGC densities for each eye and then averaged over all subjects in each experimental group.

Statistical Analysis

Student's *t*-test was used to compare GFP-expressing or SNCG-positive RGC densities and immunolabeling intensities in retinas treated with and without ILM disruption. At least six animals were included in each group for comparisons. *P* < 0.05 was considered significant.

RESULTS

Mechanical Force Is Sufficient to Disrupt the ILM of the Inner Retina

To assess the extent to which mechanical forces applied at the vitreoretinal interface in vivo could disrupt the ILM, we assessed the ILM histologically following mechanical pertur- bation of the inner retina in a rat model. Under direct visu- alization, a retractable and flexible loop with serrated edges (Fig. 1A) was used to apply force along the surface of the ILM. Multiple passes could be made along the inner retina without causing retinal detachments or vitreous hemor- rhages (Fig. 1B).

Immediately following mechanical treatment of the vitre- oretinal interface, breaks in the ILM were apparent when
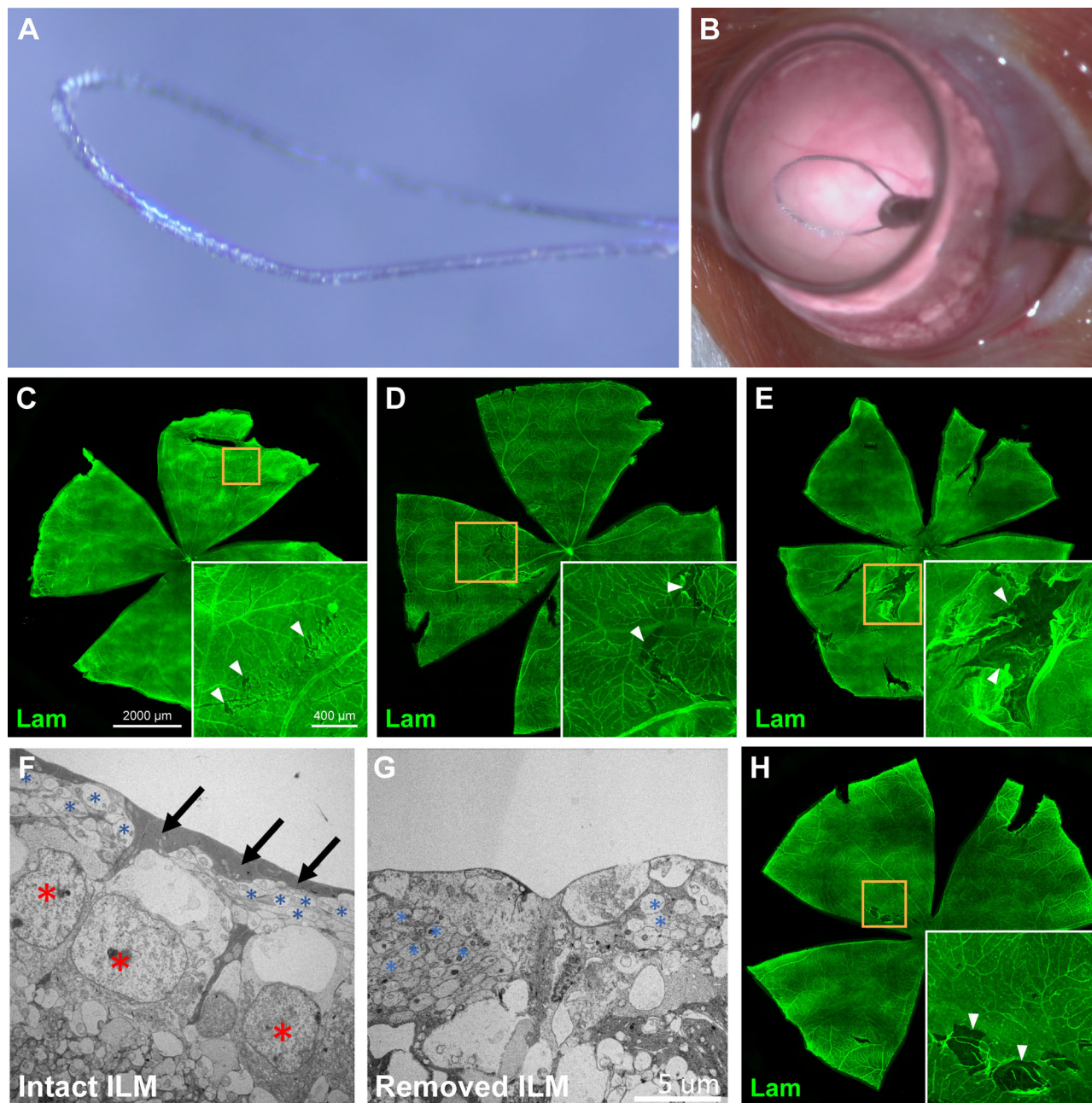

FIGURE 1. Mechanical disruption of the vitreoretinal interface removes the ILM in the rat eye. (**A**) High-magnification image of a micro- serrated nitinol loop used in human vitreoretinal surgery to create breaks in the ILM. (**B**) Intraoperative image of a micro-serrated nitinol loop being applied to the vitreoretinal surface to remove the ILM in a rat eye. (**C**) Representative image of a retinal flatmount stained for laminin immediately following ILM removal and magnified inset demonstrating small breaks (*white arrowheads*) in the ILM with conservative treatment. (**D**) Moderate treatment of the ILM creates more contiguous tears (*inset, white arrowheads*) in the ILM. (**E**) Heavy treatment can cause larger breaks (*inset, white arrowheads*) in the ILM. (**F**) Electron microscopy of the retina with an intact ILM demonstrated the presence of the ILM and Müller glia endfeet (*black arrows*) overlying axon bundles (*blue asterisks*) and cell nuclei (*red asterisks*). (**G**) In contrast, in retinas treated with mechanical disruption to remove the ILM, the ILM is absent while axon bundles (*blue asterisks*) are preserved. (**H**) Two weeks after removal of the ILM, breaks in the ILM (*inset, white arrowheads*) were still present. *Scale bars*: 2000 µm (**C–E, H**); 400 µm (*insets*, **C–E, H**); 5 µm (**F, G**).

the retina was immunolabeled for laminin, a component of the ILM. Conservative treatments of the retina resulted in focal breaks within the ILM (Fig. 1C). With more aggressive treatment, larger and confluent areas of the ILM could be displaced from the inner retina (Figs. 1D, 1E). Assessment of the inner retina and ILM by electron microscopy demonstrated complete absence of the ILM in the regions in which mechanical disruption of the ILM had been applied (Figs. 1F, 1G).

Our manipulation was applied at the vitreoretinal junction and affected the ILM and Müller cell endfeet. In theory, the Müller glia cell bodies in the inner nuclear layer were not removed and, along with ILM proteins secreted by the lens and ciliary body, could resynthesize the ILM.[14] We queried the extent to which the ILM could reform following mechanical disruption. Two weeks after mechanical disruption of the ILM, defects within the ILM continued to be observed by histological assessment (Fig. 1H).

RGC Survival Is Not Affected by Mechanical Disruption of the ILM in the Rodent

The intimate apposition of the ILM to the inner neurosensory retina poses a potential risk that mechanical disruption of the ILM could injure RGC bodies or axons and cause RGC loss. To assess this possibility, we mechanically disrupted the ILM in rats and assessed RGC survival after 2 weeks. In cross-sections of treated retinas, the cellular architecture of the inner and outer retina was intact, as demonstrated by nuclear staining and pancellular GFP expression despite the removal of the ILM (Figs. 2A–2J).

Surviving RGCs quantified in regions sampled across the entire retina did not demonstrate significant differences in the mean density of SNCG-positive RGCs between retinas in which the ILM had been disrupted (2021.8 ± 87.3 cells/mm^2) and retinas in which a flexible loop was introduced into the vitreous without contacting the ILM (2102.4 ± 118.8 cells/mm^2) ($n = 6$, $P = 0.598$). To increase the sensitivity to detect any effect that mechanical disruption of the ILM may have on RGC survival, RGC densities were also quantified only in regions of the retina in which the ILM had been disrupted. Such targeted quantification of mean RGC densities did not demonstrate a significant difference between retinal regions in which the ILM was disrupted (2406.0 ± 225.8 cells/mm^2) and the ILM was intact (2544.0 ± 251.1 cells/mm^2) ($n = 6$, $P = 0.340$) (Fig. 2K).

The health of the RGCs following mechanical disruption of the ILM was also assessed based on the intensity of SNCG immunofluorescence. There was no significant difference in SNCG fluorescence intensity between RGCs from retinas in which the ILM was intact (113.3 ± 2.1 mean pixel intensity) and retinas in which the ILM had been disrupted (108.6 ± 9.1 mean pixel intensity) ($n = 6$, $P = 0.638$) in regions sampled across the entire retina. Similarly, quantification of RGC SNCG fluorescence intensity in targeted retinal areas in which the ILM was disrupted (112.1 ± 28.3 mean pixel intensity) was not different from areas with an intact ILM (111.9 ± 29.4 mean pixel intensity) ($n = 6$, $P = 0.340$) (Fig. 2L).

Mechanical Disruption of the ILM Causes Transient Glial Activation in the Retina

To assess the degree to which an immune response in the retina might occur after mechanical disruption of the ILM, we evaluated the retinas of rodent eyes that received ILM treatments for a glial response over a time course. In control eyes with an intact ILM, CD11b-positive glial cells could be observed associated with the retinal vasculature (Figs. 3A–3C). One day following mechanical disruption of the ILM, an increased number of CD11b-positive cells that clustered within the areas of disrupted ILM were observed (Figs. 3D–3F). ILM disruption also induced local microglial cells to undergo morphological changes and adopt ameboid morphologies that contrasted with ramified morphologies of resting microglia (See Supplementary Fig. S1). The activation of CD11b-positive cells was transient, as clustering of CD11b-positive cells in areas with disrupted ILM were not observed at either 3 days (Figs. 3G–3I) or 5 days (Figs. 3J–3L) after ILM disruption.

Mechanical Disruption of the ILM Improves the Transduction Efficiency of Intravitreally Injected AAV

To evaluate whether mechanical disruption of the ILM improved viral access to the inner retina, intravitreal injections of GFP expressing AAV2 were performed in rodent eyes in which the ILM was mechanically disrupted (Figs. 4A–4H). Using an intravitreal AAV injection comprised of 5E8 vg, we observed a fivefold increase in the number of RGCs transduced to express GFP in eyes in which the ILM was disrupted (321.4 ± 61.1 cells/mm^2) compared to eyes in which the ILM was left intact (61.2 ± 41.3 cells/mm^2) ($n = 6$, $P = 0.004$) when quantified over the entire retina. When AAV transduction efficiency was quantified specifically in high GFP-expressing regions corresponding to the nasal retina that was treated with disruption of the ILM and closer to the viral injection site, we observed a fourfold increase in the number of RGCs expressing GFP in eyes in which the ILM was disrupted (1380.0 ± 290.1 cells/mm^2) compared to eyes in which the ILM was left intact (442.0 ± 249.3 cells/mm^2) ($n = 6$, $P = 0.034$) (Fig. 4I).

The intensity of GFP expression in AAV-transduced RGCs was similar in retinas with the ILM disrupted (42.2 ± 6.0 mean pixel intensity) and retinas with an intact ILM (45.6 ± 6.7 mean pixel intensity) ($n = 6$, $P = 0.712$). Comparison of RGC GFP intensity in focal areas within the retina in which the ILM was disrupted (37.3 ± 7.2 mean pixel intensity) and the ILM was intact (59.0 ± 9.3 mean pixel intensity) did not find them to be statistically significant ($n = 6$, $P = 0.098$) (Fig. 4J).

Mechanical Disruption of the ILM Permits Induced Pluripotent hRGCs to Integrate With the Neurosensory Retina

Having demonstrated that mechanical disruption of the ILM enhances access to the inner neurosensory retina of an intravitreally delivered vector, we next asked whether mechanical disruption of ILM was sufficient to promote the integration of transplanted RGCs with the host neurosensory retina. In ex vivo retinal explants in which the ILM was left intact, hRGCs transplanted directly onto the inner retina surface extended processes along the surface of the retinal explant but failed to extend processes into the inner retinal layers (Fig. 5A). Following disruption of the ILM, transplanted hRGCs could be observed extending processes under the ILM and along the retinal
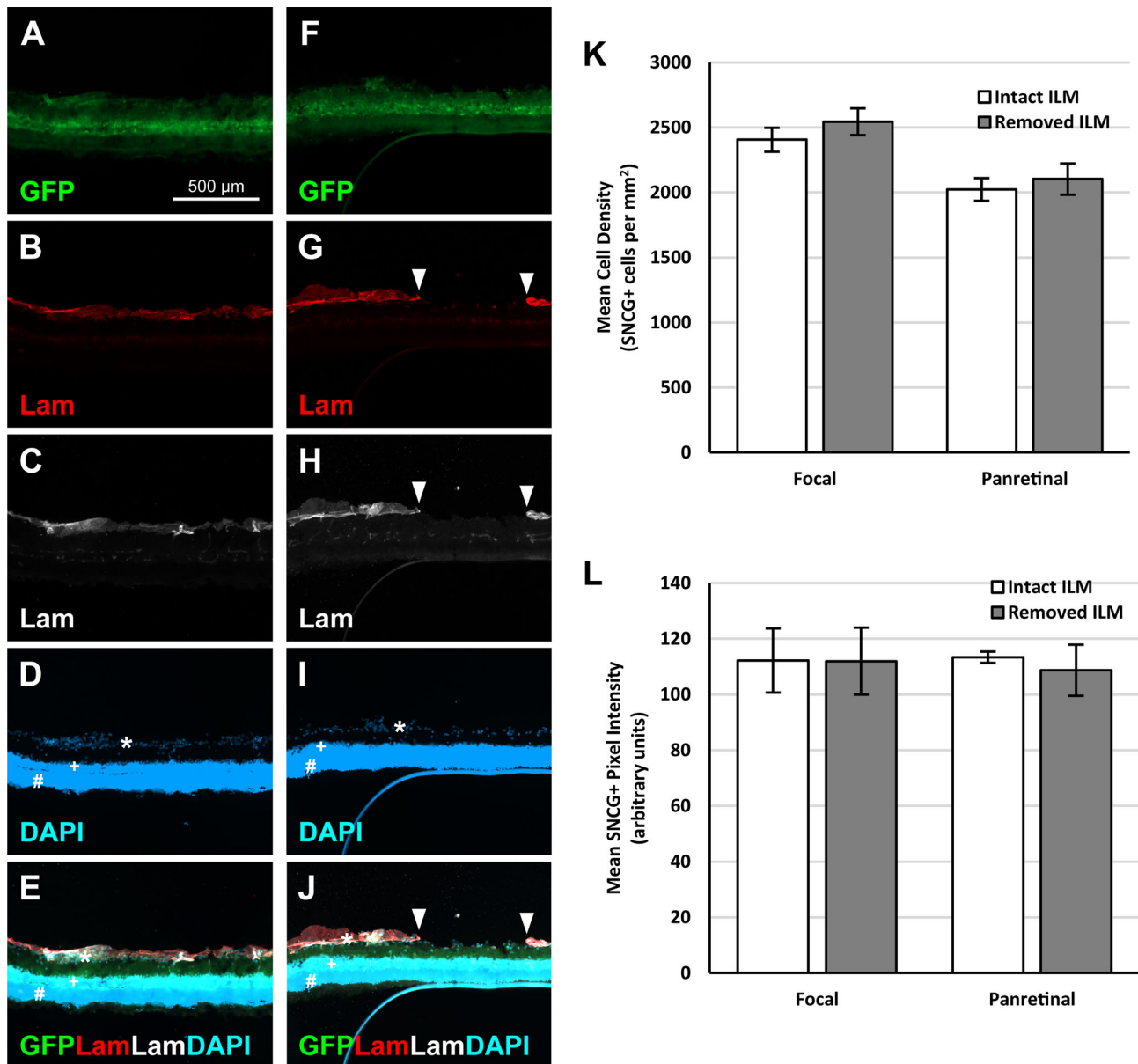
FIGURE 2. Inner retinal cellular organization is maintained following mechanical removal of the ILM in the rat eye. Representative cross-sectional images of retinas without and with removal of the ILM from rats that ubiquitously express GFP. (**A**) Naïve animals express GFP in all layers of the retina. (**B**, **C**) Immunolabeling for laminin using two different antibodies demonstrated a continuous layer of immunopositivity along the inner retinal surface. (**D**) Nuclear staining with 4′,6-diamidino-2-phenylindole (DAPI) highlights the ganglion cell (*), bipolar (+), and photoreceptor (#) cell layers. (**E**) Merged image demonstrating the retinal histology with an intact ILM. (**F**) Mechanical removal of the ILM in retinas from GFP-expressing rats does not distort the gross anatomy of the retina. (**G**, **H**) Two different antibodies that immunolabel laminin demonstrated fragmentation of the ILM (*white arrowheads*) following mechanical treatment. (**I**) DAPI staining of cell nuclei demonstrated retention of all cellular layers (ganglion cell [*], bipolar [+], and photoreceptor [#] cell layers) in the setting of ILM removal. (**J**) Merged image of immunolabeled retina following ILM removal demonstrating successful removal of the ILM with preservation of the inner retinal structures. (**K**) Quantification of RGC survival based on the density of SNCG immunolabeled cells demonstrated similar RGC densities in retinas with intact ILMs and following ILM removal in focal areas where the ILM was removed and over the entire retina. (**L**) Quantification of RGC SNCG intensity was also similar among groups, suggestive of comparable cell viabilities. *Error bars* represent SE; $n = 6$ animals per group. *Scale bars*: 500 μm.

nerve fiber layer (Fig. 5B). Additionally, in some instances, transplanted hRGC-derived processes were present in the ganglion cell layer, inner plexiform layers, and bipolar layer (Fig. 5C). At this early time point, immunohistological markers for synapses between the transplanted hRGCs and retinal explant were not observed (data not shown).

DISCUSSION

These studies demonstrate the feasibility of mechanically disrupting the ILM in the in vivo rat eye without adversely affecting the underlying retinal anatomy. Using this approach, the ILM can be targeted at specific retinal locations and the extent of ILM disruption can be
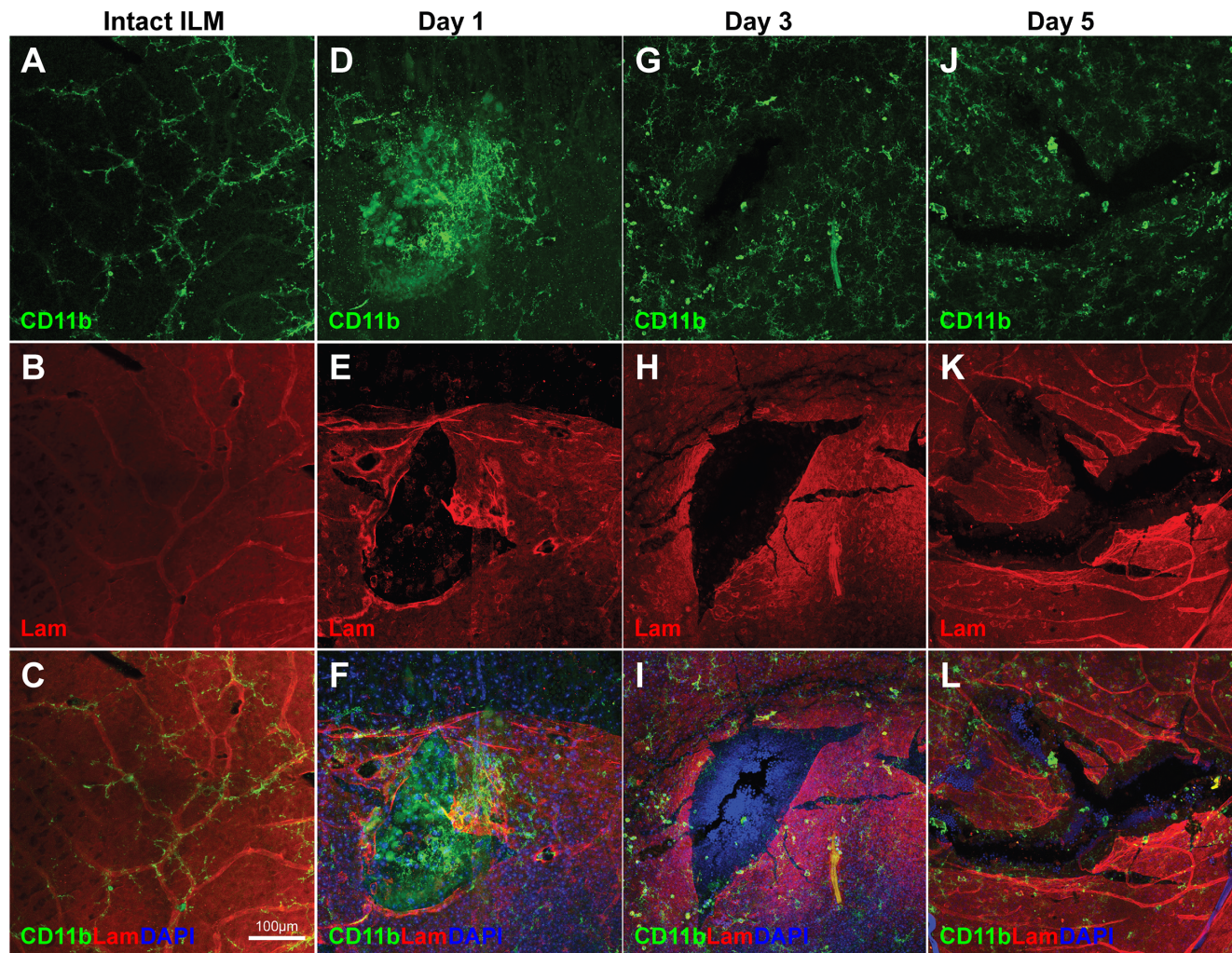
FIGURE 3. Transient glial activation occurs in the retina following mechanical removal of the ILM in the rat eye. Representative images of immunolabeled inflammatory cells in retinal flatmounts from eyes in which the ILM was left intact or mechanically disrupted. (**A–C**) In retinas with an intact ILM, CD11b-positive glial cells were loosely distributed along the retinal vasculature and adopted ramified morphologies. (**D–F**) One day after mechanical disruption of the ILM, there was an increase in CD11b-positive immunolabeling in areas where the ILM had been disrupted (as demonstrated by the lack of laminin immunolabeling), and immunolabeled glial cells could be seen adopting ameboid morphologies. (**G–I**) By day 3 after ILM disruption, CD11b-positive immunolabeling in areas of ILM disruption was significantly reduced, and clustering of the glial cells was no longer obvious. (**J–L**) Five days after ILM disruption, a majority of CD11b-positive cells within the area of ILM disruption had reverted back to assuming ramified morphologies. *Scale bar*: 100 µm.

titrated. Mechanical disruption of the ILM is sufficient to enhance the transduction efficiency of intravitreally delivered viral vectors by fivefold. Additionally, this mechanical-based approach is sufficient to remove the ILM as a physical barrier and permit transplanted RGCs to integrate with the host retina.

Direct cellular replacement of RGCs is a potential approach to vision restoration. Attempts to introduce new RGCs into the retina using intravitreal injections have demonstrated that transplanted RGCs have the potential to integrate with the retina; however, the rate of successful integration using current techniques is only about 10% of injected eyes.[7] By removing the ILM and allowing transplanted RGCs to integrate into the inner retina, it may be possible to improve the success rates of direct cellular replacement and survival of transplanted cells. Additionally, intravitreal viral vector injections can be used to treat retinal diseases. By first removing the ILM, lower titers could be

used to achieve therapeutic concentrations and avoid inflammatory reactions that can be associated with higher viral titers.

Alternative methods to remove the rodent ILM have been described. After treating retinal explants with enzymes to digest components of the ILM such as laminin and collagen, RGCs cocultured on the treated retinal explants extend processes into the inner retina.[17] Nonspecific proteases to digest the ILM also enhance the transduction efficiency of subsequently intravitreally injected viral vectors.[11] Intravitreal injections of sodium bicarbonate to liquefy the vitreous prior to interventions have also been reported.[24] These approaches, however, are unable to target specific regions of the retina and have the potential to cause off-target effects due to their nonspecific nature. This lack of specificity may cause potential complications, such as retinal hemorrhages, inflammation, and activation of the immune response, and present challenges with clinical translation
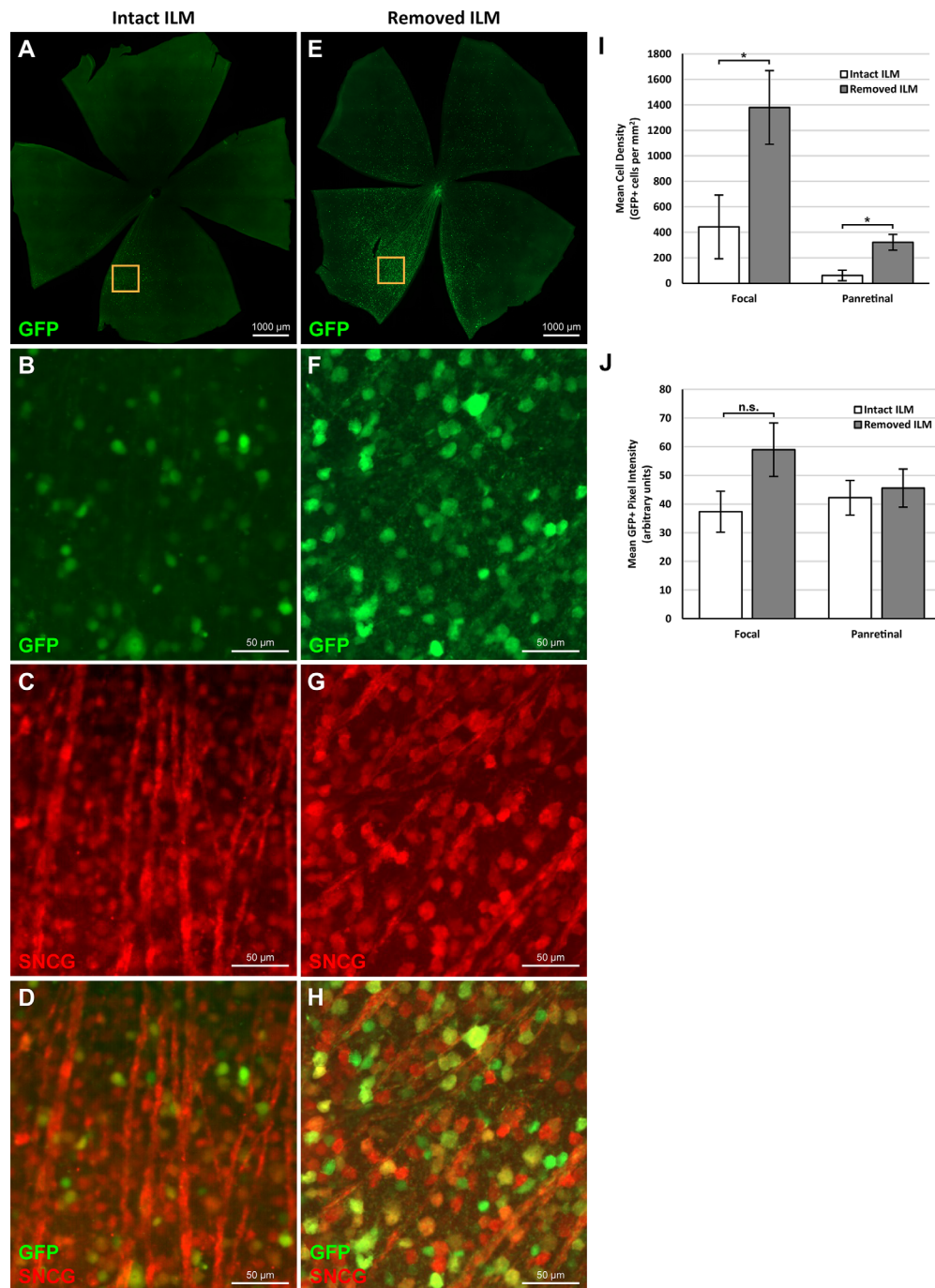
FIGURE 4. Viral transduction of RGCs by intravitreal injection is enhanced by mechanical removal of the ILM. Representative images of retinal flatmounts from eyes that received an intravitreal injection of GFP-expressing AAV2 with an intact ILM (**A**) or mechanical treatment to disrupt the ILM (**E**). Immunolabeling demonstrated that a greater number of RGCs transduced to express GFP in an eye in which the ILM is disrupted (**F**) compared to an eye in which the ILM is intact (**B**). Immunolabeling for SNCG demonstrated similar SNCG-positive RGC densities in an eye with an intact ILM (**C**) and with the ILM removed (**G**). Merged image from an eye with an intact ILM (**D**) and with the ILM removed (**H**) demonstrating colocalization of GFP and SNCG expression. (**I**) Quantification of GFP-positive cell densities demonstrated a greater number of transduced RGCs densities in retinas following ILM removal compared to retinas with intact ILMs in focal areas where the ILM was removed and over the entire retina. (**J**) Quantification of RGC GFP intensity was not statistically significant between retinas with intact ILMs and following ILM removal, although there was a trend toward greater GFP intensity in focal areas where the ILM was removed. *$P < 0.05$, Student's *t*-test. *Error bars* represent SE, $n = 6$ animals per group. *Scale bars*: 1000 µm (**A**, **E**); 50 µm (**B–D**, **F–H**).

to human patients. Additionally, the narrow therapeutic windows of these approaches are a barrier to clinical application. In contrast, mechanical removal of the ILM in human patients is already a routinely performed surgery by vitre-

oretinal surgeons in the setting of epiretinal membrane peels, macular holes, and vitreomacular traction. Mechanical disruption of the ILM may also be targeted to include only the macula to restore high-acuity central vision and
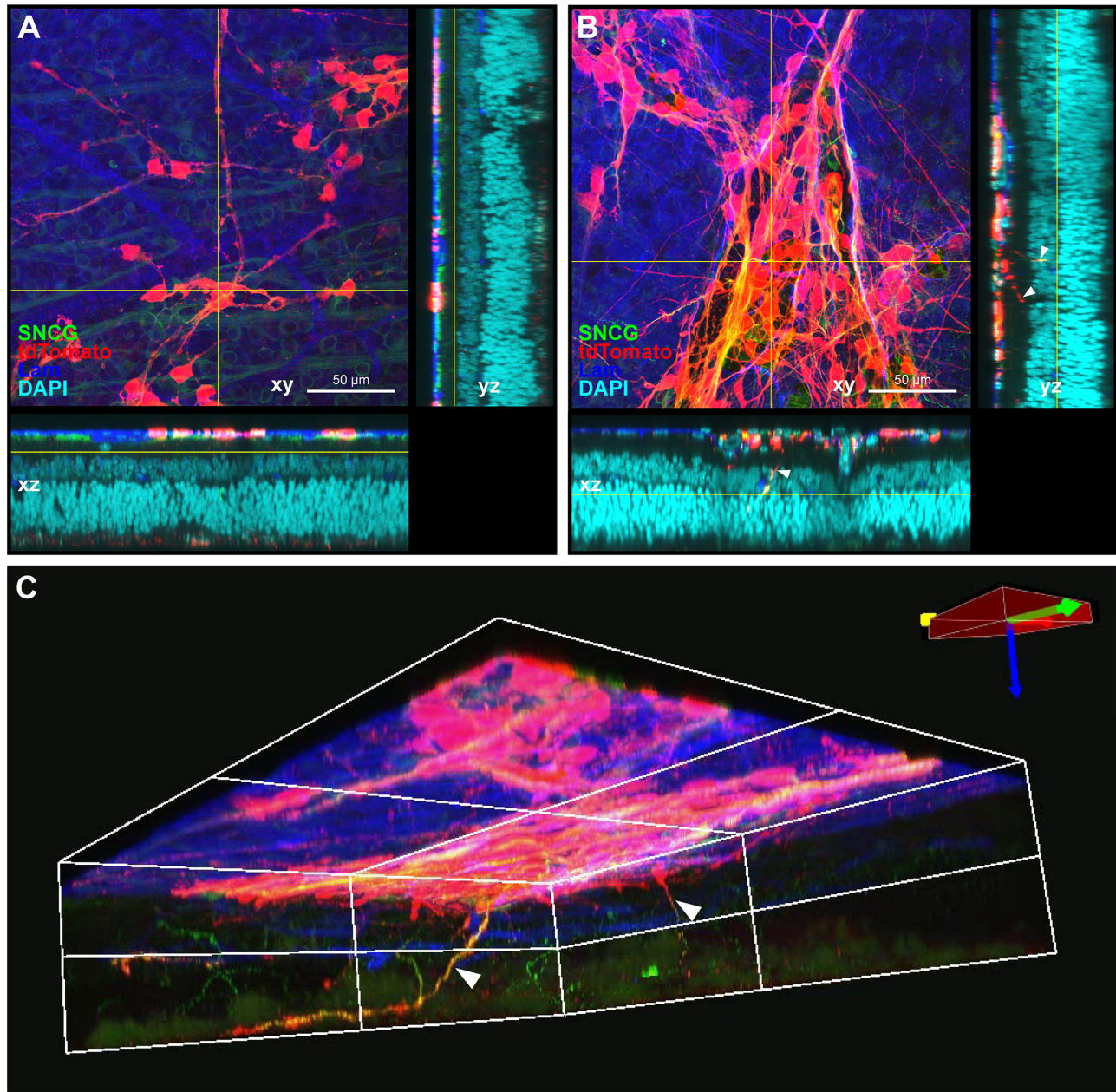
FIGURE 5. Mechanical removal of the ILM allows transplanted RGCs to integrate into the inner retina. (**A**) Confocal image of a retinal explant with an intact ILM demonstrated by laminin immunolabeling (*blue*) cocultured with human stem cell-derived RGCs that express tdTomato (*red*). Transplanted RGCs are observed on top of the ILM without penetration into the inner retina or host ganglion cell layer. (**B**) Confocal image of a retinal explant in which the ILM has been removed cocultured with hRGCs (*red*). Transplanted RGCs can be observed in the ganglion cell layer and extend process (*white arrowhead*) in the inner plexiform layer and bipolar cell layer. (**C**) Three-dimensional reconstruction from confocal images of a retinal explant in which the ILM has been removed and hRGCs have been cultured on the inner retinal surface. Transplanted RGC-derived processes (*white arrowheads*) are shown extending into outer retinal layers. This was not observed with retinal explants in which the ILM was left intact (not shown).

avoid potential complications that could arise by involving the peripheral retina. Therefore, combining mechanical ILM removal with direct RGC transplantation to enhance cell integration or with intraocular viral vector delivery to improve transduction efficiency has a greater degree of feasibility.

There are caveats and limitations to our studies. Retinal explants were used to assess the integration of transplanted RGCs in the setting of ILM removal but are not completely representative of the in vivo eye. Although this

approach allowed for the approximation of transplanted RGCs to the inner retina and leveraged gravitational forces to enhance transplant–host apposition, it does not address the poorly vascularized, inhospitable vitreous cavity in which cells transplanted into the whole eye must first survive or the other barriers to RGC replacement, such as transplant viability, axon guidance, axon targeting, synapse formation, and myelination. Also, compared to humans, rodents lack a macula, and species differences in vitreomacular anatomy may limit clinical translatability of our findings. Therefore, it

will be important to verify that removal of the ILM in nonhuman primates can similarly enhance delivery of agents or cells to the inner retina.[25] The area of ILM removed from the retina in our experiments was isolated to a single quadrant. This decision was made intentionally to minimize confounding variables such as the immune responses or inflammatory reactions from inadvertent violation of the lens capsule. Expanding the treated retina to include the entire nasal hemisphere and the temporal hemisphere through a nasal sclerotomy is technically possible but was not necessary to address the questions in our study. Additionally, although retinal structures were grossly preserved on EM following ILM removal, there may be subtle functional deficits such as microscotomas from trauma to the retinal nerve fiber layer. Lastly, retinal explants were prepared from eyes in which the RGCs were intact prior to isolation. In instances where there is a loss of RGCs, there may be histological changes that are not accounted for in this model.

To the best of our knowledge, this is the first study to describe removal of the ILM by mechanical means in an in vivo rodent model and assess the effects of mechanical ILM removal on potential therapeutic interventions. Transduction of RGCs by intravitreally injected viral vectors and the integration of transplanted RGCs into the retina are enhanced by the removal of the ILM through mechanical manipulation alone. Whether these findings can be translated to pathological eyes with the extracellular and cellular differences that occur in chronic disease states is unclear at this time.

References

1. Inoue T, Hosokawa M, Morigiwa K, Ohashi Y, Fukuda Y. Bcl-2 overexpression does not enhance in vivo axonal regeneration of retinal ganglion cells after peripheral nerve transplantation in adult mice. *Journal of Neuroscience*. 2002;22:4468–4477.

2. Weinreb RN, Aung T, Medeiros FA. The pathophysiology and treatment of glaucoma: a review. *JAMA*. 2014;311:1901–1911.

3. Sluch VM, Chamling X, Liu MM, et al. Enhanced stem cell differentiation and immunopurification of genome engineered human retinal ganglion cells. *Stem Cells Transl Med*. 2017;6:1972–1986.

4. Sluch VM, Davis CO, Ranganathan V, et al. Differentiation of human ESCs to retinal ganglion cells using a CRISPR engineered reporter cell line. *Sci Rep*. 2015;5:1–17.

5. Vergara MN, Flores-Bellver M, Aparicio-Domingo S, et al. Three-dimensional automated reporter quantification (3D-ARQ) technology enables quantitative screening in retinal organoids. *Development*. 2017;144:3698–3705.

6. Fligor CM, Langer KB, Sridhar A, et al. Three-dimensional retinal organoids facilitate the investigation of retinal ganglion cell development, organization and neurite outgrowth from human pluripotent stem cells. *Sci Rep*. 2018;8:14520.

7. Venugopalan P, Wang Y, Nguyen T, Huang A, Muller KJ, Goldberg JL. Transplanted neurons integrate into adult retinas and respond to light. *Nat Commun*. 2016;7: 10472.

8. Wu Y-R, Hashiguchi T, Sho J, Chiou S-H, Takahashi M, Mandai M. Transplanted mouse embryonic stem cell–derived retinal ganglion cells integrate and form synapses in a retinal ganglion cell-depleted mouse model. *Invest Ophthalmol Vis Sci*. 2021;62:26.

9. Hertz J, Qu B, Hu Y, et al. Survival and integration of developing and progenitor-derived retinal ganglion cells following transplantation. *Cell Transplant*. 2014;23:855–872.

10. Oswald J, Kegeles E, Minelli T, Volchkov P, Baranov P. Transplantation of miPSC/mESC-derived retinal ganglion cells into healthy and glaucomatous retinas. *Mol Ther Methods Clin Dev*. 2021;21:180–198.

11. Dalkara D, Kolstad KD, Caporale N, et al. Inner limiting membrane barriers to AAV-mediated retinal transduction from the vitreous. *Mol Ther*. 2009;17:2096–2102.

12. Heegaard S, Jensen OA, Prause JU. Structure and composition of the inner limiting membrane of the retina. SEM on frozen resin-cracked and enzyme-digested retinas of *Macaca mulatta*. *Graefes Arch Clin Exp Ophthalmol*. 1986;224:355–360.

13. Uechi G, Sun Z, Schreiber EM, Halfter W, Balasubramani M. Proteomic view of basement membranes from human retinal blood vessels, inner limiting membranes, and lens capsules. *J Proteome Res*. 2014;13:3693–3705.

14. Halfter W, Dong S, Dong A, Eller AW, Nischt R. Origin and turnover of ECM proteins from the inner limiting membrane and vitreous body. *Eye (Lond)*. 2008;22:1207–1213.

15. Halfter W, Sebag J, Cunningham ET, II. Vitreoretinal interface and inner limiting membrane. In: Sebag J, ed. *Vitreous*. New York: Springer; 2014:165–191.

16. Gui W, Pan B, Sadun AA, Sebag J. Importance of the inner limiting membrane in adults. *Exp Eye Res*. 2021;207: 108582.

17. Zhang KY, Tuffy C, Mertz JL, et al. Role of the internal limiting membrane in structural engraftment and topographic spacing of transplanted human stem cell-derived retinal ganglion cells. *Stem Cell Reports*. 2021;16:149–167.

18. Madi HA, Masri I, Steel DH. Optimal management of idiopathic macular holes. *Clin Ophthalmol*. 2016;10:97–116.

19. Ducloyer JB, Ivan J, Poinas A, et al. Does internal limiting membrane peeling during epiretinal membrane surgery induce microscotomas on microperimetry? Study protocol for PEELING, a randomized controlled clinical trial. *Trials*. 2020;21:500.

20. Johnson TV, Martin KR. Development and characterization of an adult retinal explant organotypic tissue culture system as an in vitro intraocular stem cell transplantation model. *Invest Ophthalmol Vis Sci*. 2008;49:3503–3512.

21. Johnson TV, Bull ND, Martin KR. Organotypic explant culture of adult rat retina for in vitro investigations of neurodegeneration, neuroprotection and cell transplantation. *Protoc Exch*. 2011;1–28.

22. Patel AK, Broyer RM, Lee CD, et al. Inhibition of GCK-IV kinases dissociates cell death and axon regeneration in CNS neurons. *Proc Natl Acad Sci USA*. 2020;117:33597–33607.

23. Uphoff CC, Drexler HG. Detection of Mycoplasma Contaminations. In: Helgason CD, Miller CL, eds. *Basic Cell Culture Protocols*. Totowa, NJ: Humana Press; 2013.

24. Mortada A. Chemical vitrectomy: change of solid gel vitreous to sol for vitrectomy by changing pH of vitreous toward the slight acid side. *Ann Ophthalmol*. 1982;14:465–466, 468–469.

25. Breazzano MP, Fang HS, Robinson MR, Abraham JL, Barker-Griffith AE. Vitreomacular attachment ultrastructure and histopathological correlation. *Curr Eye Res*. 2016;41:1098–1104.